Journal of Integrative Neuroscience

J. Integr. Neurosci. **2026**; 25(1): 48581
https://doi.org/10.31083/JIN48581

Original Research

The Icelandic Mutation in the Murine APP Gene, mAPP^{A673T}, on Amyloid-β Plaque Burden in the 5×FAD Alzheimer Model

Anne Anschuetz[1], Renny Listyono[1], Thomas Vorley[1], Bettina Platt[1], Charles R. Harrington[1,2], Gernot Riedel[1,*,†], Karima Schwab[1,*,†]

[1]School of Medicine, Medical Sciences and Nutrition, University of Aberdeen, Foresterhill, AB25 2ZD Aberdeen, UK
[2]TauRx Therapeutics Ltd., AB24 5RP Aberdeen, UK
*Correspondence: g.riedel@abdn.ac.uk (Gernot Riedel); karima.schwab@abdn.ac.uk (Karima Schwab)
[†]These authors contributed equally.

Academic Editor: Andrei Surguchov
Submitted: 26 November 2025 Revised: 16 December 2025 Accepted: 31 December 2025 Published: 22 January 2026

Abstract

Background: The protective Icelandic mutation in the amyloid precursor protein (*APP*) gene, APP^{A673T}, identified in Icelandic and other Nordic populations is associated with a significantly lower risk of developing Alzheimer's disease (AD). Conflicting results have been reported for the human APP^{A673T} mutation in various knock-in models of AD, but the effect of the mouse APP^{A673T} form in 5× familial AD (5×FAD) mice has never been investigated. **Methods**: We crossed C57Bl6/J mice expressing a single point mutation edited into the murine *APP* gene via Clustered Regularly Interspaced Short Palindromic Repeats–CRISPR-associated (CRISPR-Cas) gene editing, termed mAPP^{A673T}, with 5×FAD mice that overexpress human APP carrying the Swedish (K670N/M671L), Florida (I716V), and London (V717I) mutations as well as human presenilin-1 (PS1) with two mutations (M146L and L286V); the resulting mice were termed 5×FAD × mAPP^{A673T} mice. We investigated amyloid beta-protein (Aβ) pathology in 5×FAD × mAPP^{A673T}, 5×FAD and their respective controls, mAPP^{A673T}, and C57Bl6/J wild type mice, at 6-months of age using immunohistochemistry, immunoblotting, and enzyme-linked immunosorbent assay (ELISA). **Results**: We found a moderate yet significant reduction in Aβ plaque size in male 5×FAD × mAPP^{A673T} compared with 5×FAD mice. No differences were observed for soluble/insoluble Aβ40 and Aβ42 levels *per se*, but lower plaque count/area was found in 5×FAD × mAPP^{A673T} mice when Aβ42/Aβ40 ratios were low, suggesting a genotype-dependent sensitivity to Aβ aggregation and accumulation. **Conclusions**: The mAPP^{A673T} mutation has the potential to modify Aβ pathology in 5×FAD mice at the age of 6 months.

Keywords: amyloid-beta; Icelandic mutation; dementia; synaptic proteins; gliosis

1. Introduction

Alzheimer's disease (AD) is a progressive degenerative brain disorder affecting memory, cognition and behaviour [1]. It is the most common cause of dementia accounting for 60–70% of cases, and numbers are expected to exceed 150 million cases worldwide by 2050 [2]. Pathologically, end-stage AD is characterised by the formation of neurofibrillary tau tangles and extracellular amyloid beta-protein (Aβ) [3], and both pathologies may contribute to the neuronal dysfunction and cognitive decline observed in AD [4]. Amyloid-β is generated from the amyloid precursor protein (APP) through a series of enzymatic cleavages [5,6]. In the amyloidogenic pathway, APP is first cleaved by β-secretase to produce a secreted form of APP (sAPPβ) and a membrane-bound carboxyl terminal fragment (βCTF or C99) — the latter is further cleaved by the γ-secretase complex (a four-unit protease complex with presenilin as the catalytic subunits) to release Aβ peptides including Aβ40 and Aβ42. Both, Aβ40 and Aβ42, are neurotoxic and an increase in the Aβ42/Aβ40 ratio has been associated with a more pronounced plaque pathology due to higher oligomerization of Aβ42 [7–10]. In the non-amyloidogenic pathway, APP is cleaved by α-secretase producing sAPPα and αCTF (or C83).

Early work has revealed Aβ as the main constituent of senile plaques establishing its central role in AD pathophysiology [11–16]. Additionally, genetics and genomic studies have so far identified 52 pathogenic APP mutations including the Swedish (K670N/M671L), Florida (I716V), and London (V717I) mutations, all of which are located near the β-secretase or γ-secretase cleavage sites and are associated with increased Aβ accumulation in familial or early-onset AD (for review [17]). In addition, the Icelandic A673T mutation has recently been identified in Icelandic and Scandinavian populations and carriers have a significantly lower risk of developing AD [18]. The protective effect of the A673T mutation is believed to be primarily achieved through decreased Aβ production [19,20].

Over the past decades, several Aβ-based mouse models have been developed to study the role of Aβ in AD, such as mice carrying mutations in APP and presenilin-1 (PS1). The APP/PS1 model carries the Swedish APP mutation (K670N/M671L) and the PS1 mutation (M146V). The 5×FAD mice overexpress human APP with the Swedish

(K670N/M671L), Florida (I716V), and London (V717I) mutations, as well human PS1 with the M146L and L286V mutations and is one of the most frequently used and best characterised models of AD [21]. These mice develop robust amyloid plaque pathologies that are suggested to trigger synaptic and neuronal loss [21–24], inflammatory responses [25] and loss of synaptic proteins [26,27]. The protective effect of the human form of the Icelandic A673T mutation has been studied *in vitro* [18,28–30], *in vivo* using Aβ injection models [31], as well as humanised APP knock-in mice and rats [32,33]. However, the effect of the murine A673T mutation, mAPP^{A673T}, in transgenic APP mice remains elusive, but it has been suggested that endogenous mouse Aβ may alter human Aβ in transgenic models [34]. We therefore here performed histopathological, immunoblot and enzyme-linked immunosorbent assay (ELISA) immunoassays to access whether the introduction of mAPP^{A673T} in a 5×FAD background reduces Aβ levels and rescues subsequent Aβ pathologies *in vivo*.

2. Materials and Methods

2.1 Animals and Study Design

All animal experiments were performed in accordance with the European Communities Council Directive (63/2010/EU) with local ethical approval under the UK Animals (Scientific Procedures) Act (1986) and its amended regulations (2012), and under the project licence number PP2213334 compliant with the ARRIVE guidelines 2.0 [35]. The study was exploratory. No power calculations were performed *a priori*.

Mice were bred at our local animal facility. Heterozygous 5×FAD mice, on a black C57Bl6/J background (B6.Cg Tg (APPSwFlLon, PSEN1*M146L*L286V; 6799Vas/Mmjax, JAX MMRRC Stock# 034848)) were crossed with mice harbouring the Icelandic mutation generated by Clustered Regularly Interspaced Short Palindromic Repeats–CRISPR-associated (CRISPR-Cas) gene editing of a single nucleotide into the murine *APP* gene at position 673 on a black C57Bl6/J background, termed mAPP^{A673T} mice. Screening for potential off-target sites confirmed 4 low frequency targets (score <3.5; for comparison, A673T score is 100) with unlikely consequences on the phenotype. These were therefore not confirmed. Crosses were bred from heterozygous 5×FAD (male or female) with heterozygous mAPP^{A673T} (male or female). Ear biopsies were genotyped for the 5×FAD and the A673T mutation in the murine *APP* gene by Transnetyx Inc. (Cordova, USA) and yielded heterozygous offspring only. Mice were grouped by sex and according to one of the four genotypes: C57Bl6/J wild type (WT), mAPP^{A673T}, 5×FAD and 5×FAD × mAPP^{A673T}. A total of seventy-one male and female mice, 6- to 7-month-old, were included in the study (Table 1). Experimental mice were kept in sex- and genotype-specific litters ≥2 in stock box open housing under constant environmental conditions (20–22 °C temperature, 50–65% humidity, an air exchange rate of 17–20 changes per hour, and a 12-h light/dark cycle with lights turned on at 7 am with simulated sunrise/sunset) and *ad libitum* chow (Special Diet Services, Witham, UK) and water throughout. Mice were provided with corncob bedding, paper strips, and cardboard tubes (DBM, Edinburgh Scotland, UK) as enrichment throughout the experiment. They were kept in the same holding room throughout the study except when they were transferred to the euthanasia room for sacrifice and tissue harvest. Experimenters and care takers were blinded to the genotype of mice during maintenance and tissue collection. Following tissue collection, independent experimenters, also blinded to the genotype of mice, performed immunohistochemistry, ELISAs, and all statistical analyses relating to these measurements.

Table 1. Study groups and cohort sizes.

	Male (N)	Female (N)
WT	9	4
mAPP^{A673T}	9	9
5×FAD	17	4
5×FAD × mAPP^{A673T}	14	5
N - Total	∑ 49	∑ 22

WT, C57Bl6/J wild-type mice; mAPP^{A673T}, mice with the A673T Icelandic mutation in the murine *APP* gene; 5×FAD, five familial Alzheimer's disease mice; 5×FAD × mAPP^{A673T}, crosses carrying both the 5×FAD mutations and the murine A673T mutation; N, number of mice. Mice were 6- to 7-month-old when they were perfused for tissue collection.

2.2 Animal Perfusion and Brain Tissue Collection

Brain tissue was harvested from all seventy-one mice (Table 1). All chemicals were purchased from Merck Millipore (Burlington, MA, USA) if not otherwise stated. Mice were euthanised via intraperitoneal injections of a lethal dose of sodium pentobarbital (#08007/4034, Dolethal (200 mg/mL), Covetrus, UK) before undergoing intra-cardiac perfusion with heparinised phosphate-buffered saline (0.1 M PBS with 0.05% (v/w) heparin, pH 7.4 (#9041-08-1, Sigma-Aldrich, Darmstadt, Germany)) for 5 minutes. Skulls were dissected and whole brains retrieved. The right brain hemisphere was dissected, fixed overnight at room temperature in 10% (v/v) neutral-buffered formalin (#HT501128, Merck, Darmstadt, Germany), dehydrated and embedded in paraffin. Sagittal sections were prepared at 5 µm using a rotary microtome (HM 325, Leica Biosystems, Sheffield, UK), and mounted onto glass slides (SuperFrost^{TM}, Thermo Fisher Scientific, Lutterworth, UK). Sagittal sections were collected from regions at interaural 0.96 to 1.44 mm lateral of midline [36], and three sections were collected on one slide for each mouse and antibody. After brain removal, the left-brain hemisphere was

transferred immediately to liquid nitrogen and kept at –80 °C until used for protein extraction, ELISA and immunoblot quantification.

2.3 Aβ immunohistochemistry and Quantification of Aβ Plaques

Wax-embedded sagittal sections were stained in a sex-specific way using four immunohistochemistry staining boxes for male and two for female samples. Each box included a balanced number of all four genotypes. All chemicals were purchased from Merck Millipore (Burlington, MA, USA) unless otherwise stated. Sections were stained according to our standard protocol [37] using the VECTASTAIN® ABC-HRP kit (VECTOR laboratories #PK-4000), the ImmPACT DAB substrate (VECTOR laboratories, Newark, CA, USA #SK-4105), and the 6E10 anti-Aβ antibody (Biolegend, San Diego, CA, USA # 803004, diluted 1:1000). Images of hippocampal *cornu ammonis* (CA1), the dentate gyrus (DG), the visual cortex (CTX), the prefrontal cortex (PFC), and the cerebellum (CB) were taken using a light microscope at a 100× magnification (Axio Imager M1, Carl Zeiss, Jena, Germany) and saved as TIFF file format. Entire microscopic images were analysed using ilastik (Version 1.4.0.post1, https://www.ilastik.org) [38] and Fiji (Version 2.14.0, https://fiji.sc) [39]. The pixel and object classification tool in ilastik enabled training of the software based on a small subset of samples and then apply them to larger sets of images [38]. Models were trained to segment images into positively stained pixels and unstained background tissue or artefacts, and additionally to specifically recognise extracellular Aβ plaques. Variability in staining across different slices was accounted for by including faint, high and intermediate staining intensity images during the training process. After applying these models to all images, the percentage of positively stained area for the entire image, as well as extracellular plaques characteristics (number, size, and area) were quantified using Fiji. The total stained area (%), plaque count, average plaque size (μm^2) and plaque area (μm^2) were each analysed.

2.4 NeuN and GFAP Immunohistochemistry

Wax-embedded sagittal sections were dewaxed and stained as described above using NeuN (Millipore #mAB377 diluted 1:1000) and glial fibrillary acidic protein (GFAP) (ThermoFisher, Waltham, MA, USA #14-9892-82, diluted 1:100) antibodies. Images from CA1, DG, CTX, PFC and CB were taken, and positive area was quantified as described above (percentage of positively stained area).

2.5 Protein Extraction

All chemicals were purchased from Merck Millipore (Burlington, MA, USA) unless otherwise stated. The left hemibrains were pulverized in a liquid nitrogen prechilled stainless steel mortar and pestle (BioPulverizer, BioSpec, Oklahoma, USA) and homogenized with a pestle and hammer. RIPA lysis buffer (Thermo Fisher Scientific, #89900) containing Pierce Protease and Phosphatase Inhibitor Mini Tablets (Thermo Fisher Scientific, # A32959) and 1mM AEBSF (4-(2-aminoethyl)benzenesulfonyl fluoride hydrochloride) (Thermo Fisher Scientific #78431) were added in a ratio of 5:1 (mL buffer to mg wet tissue) and the homogenate was incubated for 30 minutes on ice with occasional agitation. After centrifugation at 19,000 g for 2 hours at 4 °C (Centrifuge 5427 R – Microcentrifuge (Eppendorf, Hamburg, Germany), using the FA-45-48-11 rotor), the supernatant (referred to as the RIPA-soluble supernatant fraction S1) was transferred into new reaction tubes. The residual pellet was homogenised in 5 volumes TBS (pH 7.6) containing 5 M guanidine hydrochloride (GuHCl) and 1mM AEBSF and incubated with mild agitation (11 rotations per minute, Multi Bio RS-24, Biosan, Riga, Latvia) for 16 hours at room temperature. After centrifugation at 15,000 g for 30 minutes at room temperature, the resultant supernatant fractions (referred to as GuHCl fraction, or RIPA-insoluble fraction or S2) was were each transferred into new tubes. AEBSF was added to both S1 and S2 extraction buffers at a 1 mM final concentration to prevent degradation of Aβ. S1 and S2 fractions were stored at –20 °C until use. Total protein concentration of S1 and S2 fractions was determined using the bicinchoninic acid (BCA) protein assay (Pierce™ BCA Protein Assay Kit, Thermo Fisher Scientific, #23225) with bovine serum albumin (BSA: 0.125–2.000 mg/mL) as a reference standard.

2.6 Aβ, Tau and Synaptic Proteins ELISA

All ELISAs were conducted according to the manufacturer's instructions, and each sample was measured in duplicates.

RIPA-soluble S1 was used to measure human Aβ40 (Invitrogen #KHB3481), human Aβ42 (Invitrogen, Waltham, MA, USA # KHB3441), mouse tau (Invitrogen #KMB7011), mouse synaptosomal associated protein 25kDa (SNAP25, MyBiosource #MBS451917), mouse syntaxin 1A (STX1A, MyBiosource #MBS452386), and mouse synaptophysin (SYP, MyBiosource #MBS453910). First, all S1 samples were diluted to a protein concentration of 4 µg/µL in RIPA (including protease and phosphatase inhibitors + AEBSF). For Aβ40 and Aβ42, S1 samples were further diluted 1:5 in dilution buffer provided within each kit. All 5×FAD and 5×FAD × $mAPP^{A673T}$ samples were used, and one WT and one $mAPP^{A673T}$ sample was included on each plate as a control. For tau, S1 samples at 4 µg/µL in RIPA were used, and quantification was conducted for all 71 mice. For synaptic proteins, S1 samples were further diluted in PBS at 1:2 for STX1A and 1:10 for SYP and SNAP25 and quantification was conducted for 70 mice (1 female WT excluded for SYP/SNAP25 due to sample preparation error). Additionally, Aβ40 and Aβ42 were quantified in GuHCl S2 fractions using the same kits as above. All S2 samples were first diluted to a protein

Table 2. List of antibodies.

Antibody	Species/Types	Immunogen	Supplier	ID	Dilution
2B3	Mouse monoclonal	Synthetic peptide in C-terminus portion of human sAPPα	IBL	11088	1:500
Poly8134	Rabbit polyclonal IgG	Soluble fragment cleaved N-terminal to the β-secretase cleavage site of APP	Biolegend	813401	1:1000
CT695	Rabbit polyclonal	Synthetic 22 amino acid peptide at APP C-Terminus	Invitrogen	51-2700	1:1000

Primary anti-Aβ antibodies used for immunoblotting.

APP, amyloid precursor protein.

concentration of 1 µg/µL in TBS (pH 7.6) containing 5M GuHCl (including protease and phosphatase inhibitors + AEBSF) and further diluted 1:1000 for Aβ40 or 1:7500 for Aβ42 using the dilution buffer provided within each kit. All 5×FAD and 5×FAD × mAPP^{A673T} samples were used, and one WT and one mAPP^{A673T} sample was included on each plate as a control.

2.7 Quantification of APP and APP Fragments by Immunoblotting

S1 RIPA-soluble samples were used for immunoblotting (4 µg/µL in RIPA buffer including protease and phosphatase inhibitors + AEBSF). All chemicals were purchased from Merck Millipore (Burlington, MA, USA) if not otherwise stated. In brief, protein extracts were mixed with 4× Laemmli sample buffer (Bio-Rad Laboratories, Hercules, CA, USA, #1610747) and incubated for 15 minutes at 37 °C. Twenty µg protein per lane was loaded onto stain-free 4–15% gradient glycine gels (Bio-Rad Laboratories #4568086) and a protein standard (Bio-Rad Laboratories # 1610376) was loaded onto each gel as molecular weight (MW) marker. Proteins were separated in Tris-glycine-buffer (192 mM glycine, 25 mM Tris and 0.9% (w/v) SDS) at 100 V for around 2 hours on ice using a Mini-PROTEAN Electrophoresis Cell (Bio-Rad Laboratories). Proteins were transferred to methanol-activated PVDF membranes (Bio-Rad Laboratories #1620177) at 5V for 30 minutes in Towbin transfer buffer (25 mM Tris, 200 mM glycine, 0.1% (w/v) SDS and 20% (v/v) ethanol). Membranes were then blocked for 1 h at RT in blocking solution (4% (w/v) BSA) in TBS-T (TBS with 0.2% (v/v) Tween-20) and incubated overnight at 4 °C in 5 mL primary antibody (Table 2) diluted in blocking solution. The next day, membranes were washed 3 × 10 minutes in TBS-T and incubated for 1 h at RT in 25 mL secondary antibody (goat anti-mouse IgG, Bio-Rad Laboratories #5178-2504, or goat anti-rabbit IgG, Bio-Rad Laboratories #5196-2504, 1:5000) diluted in blocking solution containing StrepTactin-HRP conjugate (Bio-Rad Laboratories #1610381; 1 µL conjugate per 100 mL blocking solution). After washing 3 × 10 minutes in TBS-T, membranes were overlaid for 1 min with ECL solution (Bio-Rad Laboratories #1705061). The chemiluminescence signals were detected by the ChemiDoc Imaging System and the Image Lab software (ChemiDoc™ XRS+ Imaging System (Bio-Rad Laboratories #1708255)) and normalised to protein loading signals using Coomassie Blue stain (0.1% Coomassie in 20% acetic acid and H_2O). A mixture of all samples was included on each gel for between-gel normalization.

2.8 Data Analysis

No *a priori* exclusion criteria were set. However, some immunohistochemistry (IHC) samples were excluded due to tissue damage during sectioning or lack of staining possibly due to sample preparation errors, and additionally some samples were excluded after immunoblotting due to damage of the gel. Details are specified in the respective sections below. Data were analysed and graphs generated in R (Version 4.4.3, R Core Team, Vienna, Austria) using linear models or generalized linear models and analysed using 2- or 3-Way ANOVA or Wald χ^2 tests. Where appropriate, post-hoc tests were performed using Bonferroni correction. For 6E10 and NeuN IHC staining, males and females were analysed separately and the effects of brain region, genotype and their interaction on each parameter were assessed. For each analysis, it was first determined whether data met assumptions for normality or if any data transformations were necessary. Data met necessary assumptions after transformation using either simple methods (square root, log) or more advanced methods (Box-Cox or Yeo-Johnson transformation). As IHC was performed over several days, a nuisance factor "Staining Day" was included in statistical models if it had a significant effect on the variable being analysed. Total 6E10-positive area showed a significant nuisance factor effect in both males and females. Meanwhile in the analysis of plaque parameters, NeuN and GFAP positive area, the staining day showed only a weak or non-significant effect and was therefore excluded as a factor. A similar approach was taken for ELISA data, where the effects of sex, genotype and their interaction on protein levels were assessed. Data were first tested for necessary assumptions and transformed if necessary. For Aβ and tau ELISA, data were transformed using either simple or more advanced methods (see above) while synaptic protein data already met assumptions for two-way ANOVA. Due to the large number of samples multiple ELISAs were performed, which in part were from different lots and performed on different days. This was accounted for by inclusion of a nuisance factor where necessary. Nuisance factor was included in S1 Aβ42 and analysis of synaptic proteins. Western blot data were analysed using one-way ANOVA with factor genotype following data transformation where

necessary (for details, see figure legends). All statistical outcomes are reported based on linear or generalised linear models of transformed data, but figures show untransformed data. Due to a sample preparation error, one sample (female WT) had to be excluded from SYP and SNAP25 ELISA. No other samples or data points were excluded from analysis. For each genotype and sex Pearson correlation matrices were generated from Aβ ELISA and Aβ IHC data and compared visually and statistically using the Jennrich test [40] to determine if the matrices were significantly different from each other. To determine whether the level of soluble or insoluble Aβ42/Aβ40 affected plaque counts and whether this effect varies between genotypes, generalized linear modelling was used. Negative binominal models were used and nested models (with or without interaction/factors) were compared using likelihood ratio tests to determine significance of each main effect (Aβ42/Aβ40 ratio and genotype) and interaction. Similarly, linear modelling was applied to determine the effect of Aβ42/Aβ40 ratio on plaque area and whether this differs between genotypes. All data are presented as mean $\pm$ standard deviation (SD) and alpha was set to $p < 0.05$.

3. Results

We have experienced increased mortality in female 5×FAD mice during cohort aging (data not shown). The survival rate (until tissue harvest) was lowest in female 5×FAD (57%) compared to all other genotypes/sexes (between 80 and 100%). The remaining experimentally used mice were generally in good health when they were investigated at the age of 6 months (normal activity, no piloerection etc.). Furthermore, body weights differed considerably between genotypes ($F_{Genotype}(3,63) = 4.86$, $p = 0.0042$) and sexes ($F_{sex}(1,63) = 133$, $p < 0.0001$). In male cohorts, 5×FAD and 5×FAD × mAPP^{A673T} were generally lighter than WT and mAPP^{A673T} mice (WT: 35.23 $\pm$ 2.59 g; mAPP^{A673T}: 35.80 $\pm$ 3.76 g; 5×FAD: 32.47 $\pm$ 3.43 g; 5×FAD × mAPP^{A673T} 33.79 $\pm$ 3.83 g). This was also the case in female cohorts (WT: 25.98 $\pm$ 0.82 g; mAPP^{A673T}: 26.93 $\pm$ 2.55 g; 5×FAD: 22.60 $\pm$ 1.45 g; 5×FAD × mAPP^{A673T} 23.20 $\pm$ 0.84 g).

3.1 Icelandic Mutation and Aβ Pathology

We proceeded to assess via IHC whether the introduction of the Icelandic mutation in a 5×FAD background changed Aβ levels using the monoclonal antibody 6E10. This antibody is widely used in AD research; it recognises APP fragments that contain the Aβ sequence (including full-length Aβ40 and Aβ42, as well as smaller fragments when used during immunoblotting) and is expected to label both intracellular and extracellular deposits of APP and Aβ. Representative micrographs of male 5×FAD and 5×FAD × mAPP^{A673T} (Fig. 1A), female 5×FAD and 5×FAD × mAPP^{A673T} (Fig. 1B), as well as WT and mAPP^{A673T} mice (**Supplementary Fig. 1A**) reveal uniform and punctate cytosolic staining (Fig. 1A,B & **Supplementary Fig. 1A**, black arrowheads) and frequent nuclear as well as occasional axonal/ dendritic staining (Fig. 1A,B & **Supplementary Fig. 1A**, white arrowheads). In WT and mAPP^{A673T} mice (**Supplementary Fig. 1A**), there were abundant 6E10-positive neurones across all cortical layers in visual cortex and PFC and especially in the pyramidal cell layer of CA1 and granular cell layer of DG. Fewer 6E10-positive cells were found in other CA1 and DG layers as well as in the hilus. In CB granule cell layer showed widespread cytoplasmic labelling while fewer positive cells were seen in the molecular layer. Additionally, large Purkinje cells were also frequently positive for 6E10 labelling. A similar cytosolic and axonal/ dendritic staining was also seen in 5×FAD and 5×FAD × mAPP^{A673T} (Fig. 1A,B).

Extracellular Aβ deposits were absent in WT and mAPP^{A673T} mice (**Supplementary Fig. 1A**), but 5×FAD and 5×FAD × mAPP^{A673T} mice of both sexes showed abundant extracellular Aβ deposits (Fig. 1A,B). These consisted of characteristic Aβ plaques with an intensely labelled core and a fainter diffuse halo (Fig. 1A,B, black arrows). In addition, deposits of smaller, intensely labelled core-only plaques with little to no halo (Fig. 1A,B, asterisk) and less intensely labelled diffuse plaques with no discernible core (Fig. 1A,B & **Supplementary Fig. 1A**, white arrows) were identified. All three types of plaques were found in hippocampal and cortical areas in 5×FAD and 5×FAD × mAPP^{A673T}, but none were seen in CB (Fig. 1A,B). Plaque number, size and area were measured to quantify extracellular Aβ deposits. These three parameters differed significantly between the four genotypes, confirming the Aβ plaque pathology phenotype in 5×FAD and 5×FAD × mAPP^{A673T} male and female crosses (**Supplementary Fig. 1B–G**, p values < 0.001). When the total 6E10 signal was quantified, these genotype differences persisted only in female but not male cohorts (**Supplementary Fig. 1H**, p not significant in males and **Supplementary Fig. 1I**, $p < 0.001$ in females). However, while the number of plaques was similar between 5×FAD and 5×FAD × mAPP^{A673T} male (Fig. 1C) and female mice (Fig. 1D), male 5×FAD × mAPP^{A673T} had significantly smaller plaques than male 5×FAD (Fig. 1E, $F_{Genotype}(1,114) = 5.24$, $p = 0.024$), but no genotype-related differences were measured for this parameter in female cohorts (Fig. 1F). The plaque area was also similar between genotypes in male (Fig. 1G) and female mice (Fig. 1H). Finally, the number of plaques varied significantly between brain regions in male 5×FAD and 5×FAD × mAPP^{A673T} males (Fig. 1C, $\chi^2_{Brain\ Region}(3) = 12.14$, $p = 0.007$), where significantly more plaques were counted in PFC than in CA1 (post-hoc test $p = 0.009$).

In summary, we have confirmed the Aβ plaque pathology phenotype in 5×FAD and 5×FAD × mAPP^{A673T} male and female cohorts and show, for males, that the mA673T mutation significantly decreases the size of Aβ plaques in 5×FAD × mAPP^{A673T} crosses compared to 5×FAD.

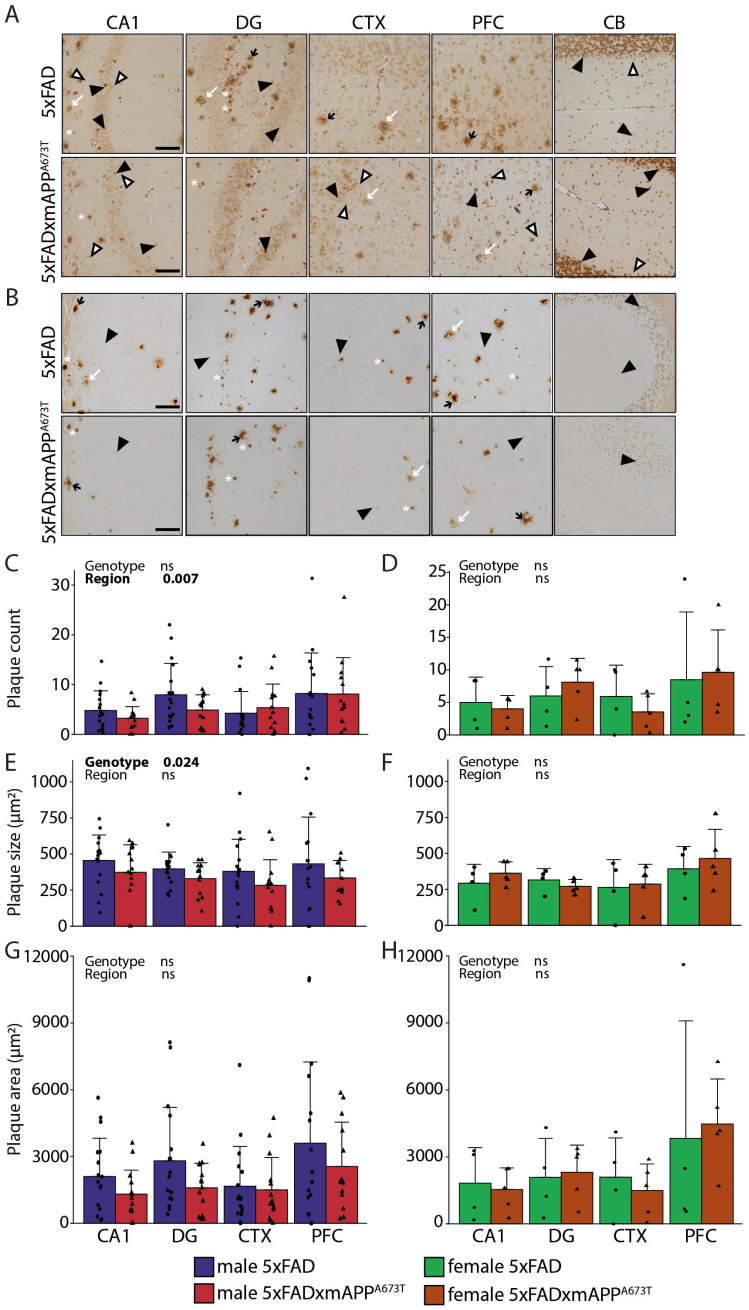

Fig. 1. Aβ immunohistochemistry using the antibody 6E10. Representative Aβ immunohistochemistry images of brain sections of male (A) and female (B) 5×FAD and 5×FAD × mAPP^{A673T} mice stained with the antibody 6E10 (Biolegend # 803004, diluted 1:1000). Images from CA1, DG, CTX and PFC were taken using a light microscope at a 100× magnification. Black arrowheads, cytosolic staining; white arrowheads, axonal/dendritic staining; black arrows, dense core plaques with halo; white arrows, small dense plaques with no/little halo; asterisk, diffuse plaques; scale bars, 100 µm. 6E10 labelling was quantified using ilastik for plaque counts (C,D), plaque size (E,F) and plaque area (G,H) in male and female 5×FAD and 5×FAD × mAPP^{A673T} mice in four brain regions. Data is shown as individual values, group mean, and S.D. Statistical analysis entailed Wald χ^2 test (C,D) or two-way ANOVA (E–H) with genotype and region as independent variables. Significance of each factor and the interaction is indicated above each graph. No data transformation was performed for plaque counts (C,D) while size and area were Box-Cox (E,F,H) or square-root transformed (G). Males: 5×FAD: n = 17 (PFC n = 16), 5×FAD × mAPP^{A673T}: n = 14 (PFC n = 13). Females: 5×FAD: n = 4, 5×FAD × mAPP^{A673T}: n = 5. Abbreviations: CA1, hippocampal CA1; CTX, visual cortex; DG, dentate gyrus; ns, not significant; PFC, prefrontal cortex; 5×FAD, 5× familial Alzheimer's disease; APP, amyloid precursor protein; SD, standard deviation.

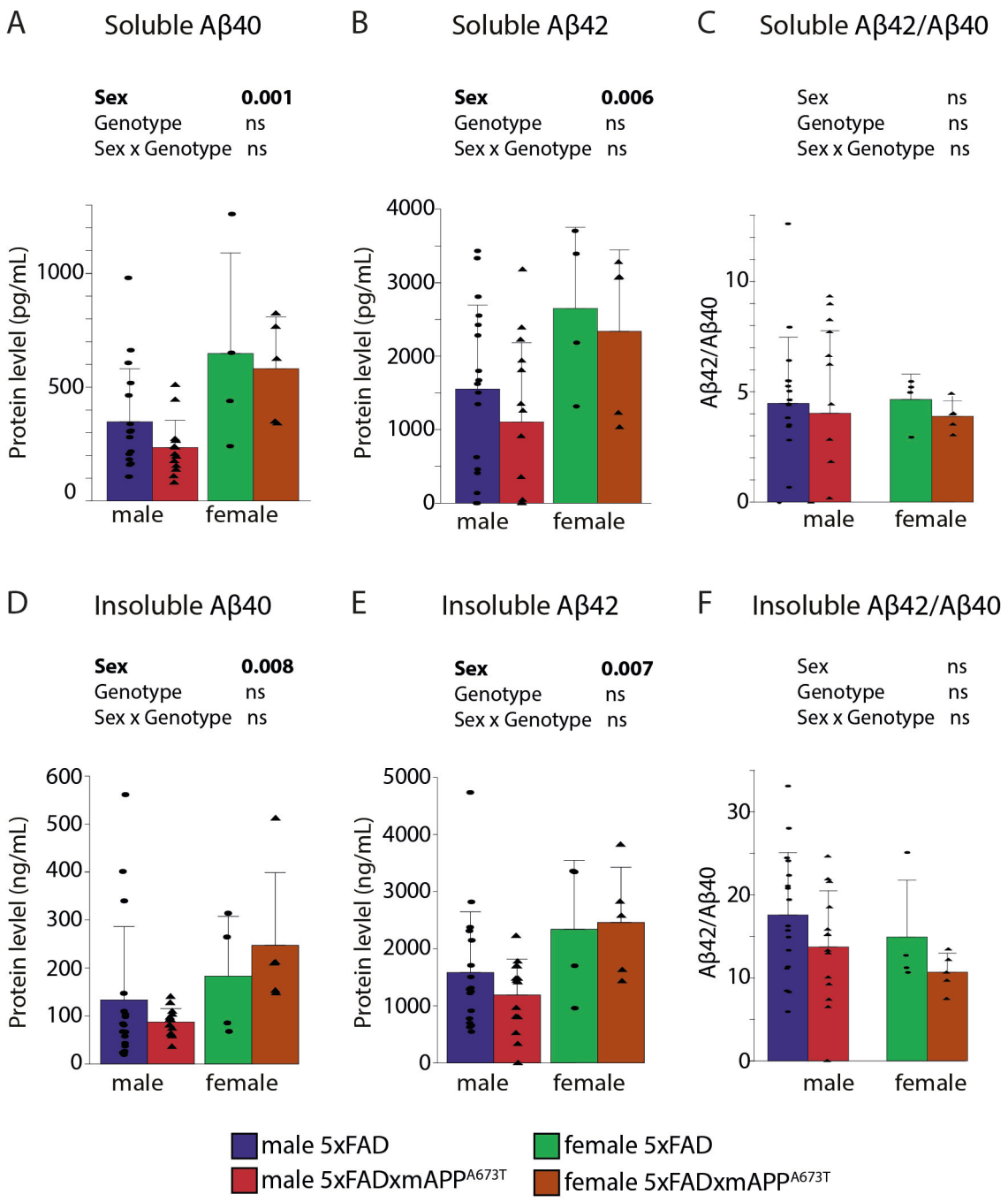

Fig. 2. Quantification of soluble and insoluble Aβ. Human Aβ40 and Aβ42 and Aβ42/Aβ40 ratios were quantified in RIPA-soluble (A–C) and insoluble fractions (D–F) in male and female WT, mAPP^{A673T}, 5×FAD and 5×FAD × mAPP^{A673T} mice. Data were analysed using two-way ANOVA with sex and genotype as independent variables. Significance of each factor and the interaction is indicated above each graph. Ratios did not require data transformation and remaining data were transformed using Yeo-Johnson (A,D) or Box-Cox (B,E) transformation. Data is shown as individual values, group mean, and S.D. Males: 5×FAD: n = 17, 5×FAD × mAPP^{A673T}: n = 14. Females: 5×FAD: n = 4, 5×FAD × mAPP^{A673T}: n = 5. One wild-type and one mAPP^{A673T} were included on each ELISA plate as a control (see Methods). Abbreviations: ns, not significant; WT, wild type.

Given this significant reduction of Aβ plaque size in male 5×FAD × mAPP^{A673T} crosses, we further explored, using ELISA, whether this led to changes in soluble and insoluble Aβ40 and Aβ42 isoforms (Fig. 2). While all 5×FAD and 5×FAD × mAPP^{A673T} samples were measured, only one WT and one mAPP^{A673T} samples were included. Both presented with very low signals, or signals below detection thresholds and confirmed the specificity of the ELISA as-

says for human Aβ (data not shown). Female 5×FAD and 5×FAD × mAPP^{A673T} crosses had almost twice as much soluble Aβ40 than their male counterparts (Fig. 2A, $F_{sex}(1,36) = 12.77$, $p = 0.001$), and this was also the case for soluble Aβ42 (Fig. 2B, $F_{sex}(1,35) = 8.35$, $p = 0.007$), while the Aβ42/Aβ40 ratio was similar between cohorts (Fig. 2C). Similarly, females of both genotypes had more insoluble Aβ40 (Fig. 2D, $F_{sex}(1,36) = 7.67$, $p = 0.008$), and Aβ42 (Fig. 2E, $F_{sex}(1,36) = 8.02$, $p = 0.007$), but again a similar Aβ42/Aβ40 ratio (Fig. 2F) compared to their male counterparts. Neither soluble, nor insoluble Aβ40 and Aβ42 nor their ratios differed between 5×FAD and 5×FAD × mAPP^{A673T} crosses, but a trend towards reduction for Aβ42/Aβ40 in S2 was observed for 5×FAD × mAPP^{A673T} compared to 5×FAD (Fig. 2F, $F_{Genotype}(1,36) = 3.31$, $p = 0.077$).

We next investigated Aβ, APP, and its metabolites using immunoblotting to assess whether the murine A673T mutation would shift the processing of the human isoforms from the amyloidogenic to the non-amyloidogenic pathway (Fig. 3 and additionally see **Supplementary Fig. 2** for uncropped images of the complete cohort). We have used three different anti-APP/Aβ antibodies (Table 2) on male cohorts as only these returned genotype-specific differences for Aβ plaques (Fig. 1).

The monoclonal antibody 2B3 is directed against the C-terminus of human sAPPα. Applying our immunoblotting protocol to RIPA-soluble S1 fractions, this antibody revealed three bands: two higher molecular weight bands at around 140 and 100 kDa (sAPPα-140 and sAPPα-100), as well as a 17-kDa fragment (Fig. 3A, see black arrowheads). The levels of these three bands, however, was similar between genotypes (Fig. 3B–D). The second antibody, Poly8134, is polyclonal and directed against APPβ. It too revealed three bands: sAPPβ-100 (MW ~100 kDa), sAPPβ-50 (MW ~50 kDa) and a 17-kDa fragment (Fig. 3E, see black arrowheads), all of which were similar across the four genotypes (Fig. 3F–H). The third antibody, CT695, reacts with CTFs of human APP and revealed four fragments: CTF75 (~75 kDa), CTF50 (~50 kDa), CTF25 (~25 kDa), and CTF19 (19 kDa, Fig. 3I, see black arrowheads). Again, all these four bands were similar in quantity between genotypes (Fig. 3J–M). All three antibodies revealed considerable cross-reactivity for murine and human APP and their metabolites (e.g., similar bands for WT and 5×FAD mice), likely because mouse and human APP differ by only three amino acids [41].

3.2 Icelandic Mutation, Tau and Synaptic Proteins

Given the synergetic and reciprocal regulatory effect of Aβ and tau, and their established role in inducing synaptic protein alterations in AD patients and AD mouse models, we have further examined whether the A673T mutation in the murine *APP* gene changes endogenous tau levels and/or rescue alterations of synaptic proteins. Mouse tau and three synaptic proteins—SYP, SNAP25, and STX1A—were measured using mouse-specific ELISAs (Fig. 4). Tau was similar across genotypes and sexes (Fig. 4A), as were SYP (Fig. 4B) and SNAP25 (Fig. 4C, all F values <1). STX1A however, was different between the 4 genotypes (Fig. 4D, $F_{Genotype}(3,62) = 3.1$, $p = 0.034$), but none of the differences reached statistical significance in *post-hoc* tests.

3.3 Icelandic Mutation and Prediction of Amyloid Pathology

Pearson correlations were generated for data from 5×FAD and 5×FAD × mAPP^{A673T} male and female mice. These correlation matrices included Aβ pathology (IHC and ELISA) and tau quantification (**Supplementary Fig. 3**, see supporting information). Correlation matrices differed significantly between male 5×FAD and 5×FAD × mAPP^{A673T} mice (**Supplementary Fig. 3A,B**, $p < 0.001$, see supporting information). Although differences were obvious between female 5×FAD and 5×FAD × mAPP^{A673T}, sample sizes were too small to compare correlation matrices statistically (**Supplementary Fig. 3C,D**, see supporting information). Overall, there was a high degree of correlation for Aβ (IHC with ELISA), especially in 5×FAD males, while almost no correlations were observed between Aβ and tau in either genotype. When only amyloid pathologies are correlated (Fig. 5A–D), we found that male 5×FAD mice showed significant positive correlations between Aβ40 and Aβ42 levels with plaque counts and plaque area which were almost entirely absent in 5×FAD × mAPP^{A673T} (Fig. 5A and Fig. 5B, see asterisks for significant correlations). Additionally, 5×FAD males showed significant negative correlations between Aβ42/Aβ40 ratio in S2 with plaque counts/area. In female mice, the Aβ42/Aβ40 ratio in S1 fraction correlated significantly with plaque count/area in 5×FAD mice, but this was not the case in 5×FAD × mAPP^{A673T} (Fig. 5C and Fig. 5D, see asterisks for significant correlations).

To further explore these differences in correlations, generalised linear modelling was used to determine whether the Aβ42/Aβ40 ratio in insoluble and soluble fractions would predict plaque count and whether this effect differs between genotypes (Fig. 5E–H). In males, independent of genotype, the Aβ42/Aβ40 ratio in S1 did not influence plaque count (Fig. 5E). By contrast, in S2, 5×FAD males showed a negative association between Aβ42/Aβ40 ratio and plaque count (Fig. 5F, $p < 0.001$). The relationship showed a positive direction in 5×FAD × mAPP^{A673T} ($p < 0.001$), resulting in lower plaque counts in 5×FAD × mAPP^{A673T} than 5×FAD males when the Aβ42/Aβ40 ratio is low, with a significant difference between both genotypes for the number of plaques which depended on Aβ42/Aβ40 (Fig. 5F, likelihood ratio test: $\chi^2(1) = 8.79$, $p = 0.003$). In 5×FAD female mice, increase in Aβ42/Aβ40 ratio in S1 was associated with a predicted decrease in plaque counts (Fig. 5G, $p < 0.001$). The opposite was the case in 5×FAD

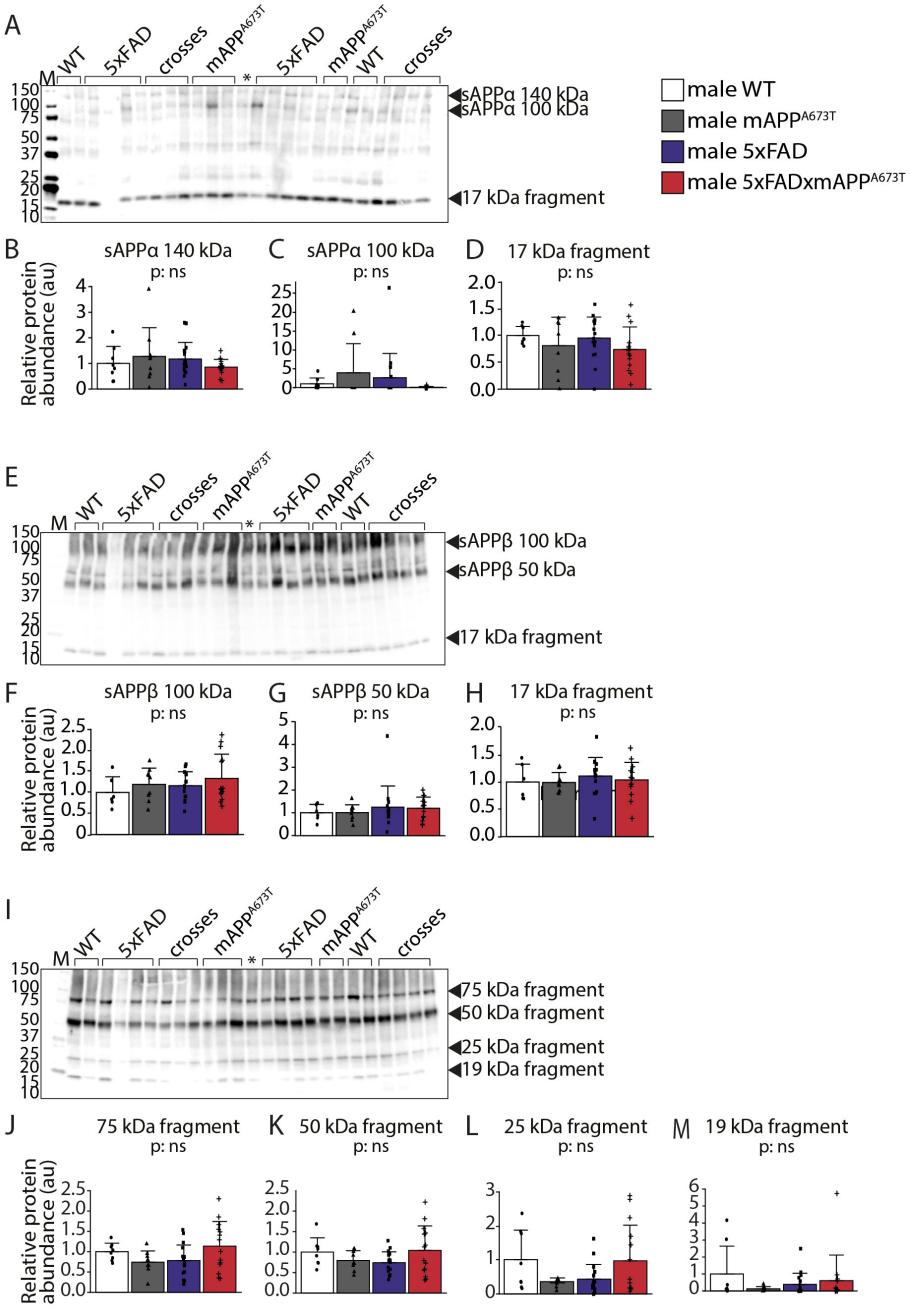

Fig. 3. Quantification of APP/Aβ species using immunoblotting. Proteins from RIPA-soluble S1 fractions were separated by SDS-PAGE (20 µg per lane) and labelled with the antibody 2B3 against sAPPα (A), Poly8134 against sAPPβ (E), and CT695 against CTFs (I). Densitometric quantification of the bands of interest (arrowheads) was conducted using the Image Lab software and normalisation to total protein loading. For antibody 2B3, three bands at 10 kDa (B), 100 kDa (C) and 17 kDa (D) were identified. For the antibody Poly8134, three bands were quantified at 100 kDa (F), the 50 kDa (G) and 17 kDa (H). The third antibody, CT695 revealed four bands at 75 kDa (J), 50 kDa (K), 25 kDa (L) and 19 kDa (M). Data is shown as individual values, group mean, and SD Data were analysed using 1-way ANOVA with genotype as independent variable and significance is indicated above each graph. No data transformation was required. Males: WT: n = 8 (n = 6 for Poly8134 antibody), mAPP^{A673T}: n = 9, 5×FAD: n = 17 (n = 15 for Poly8134 antibody), 5×FAD × mAPP^{A673T}: n = 14. Abbreviations: crosses, 5×FADx mAPP^{A673T}; ns, not significant; *: loading control.

× mAPP^{A673T} females, with increasing Aβ42/Aβ40 values associated with an increase in plaque counts (Fig. 5G, p = 0.001). This resulted in lower predicted plaque counts in 5×FAD × mAPP^{A673T} compared to 5×FAD females for low values of Aβ42/Aβ40, and a significant difference between genotypes in the prediction of plaque count based on the Aβ42/Aβ40 ratio (Fig. 5G, likelihood ratio test: χ^2 (1) = 7.52, p = 0.0061). The Aβ42/Aβ40 ratio in S2 was not

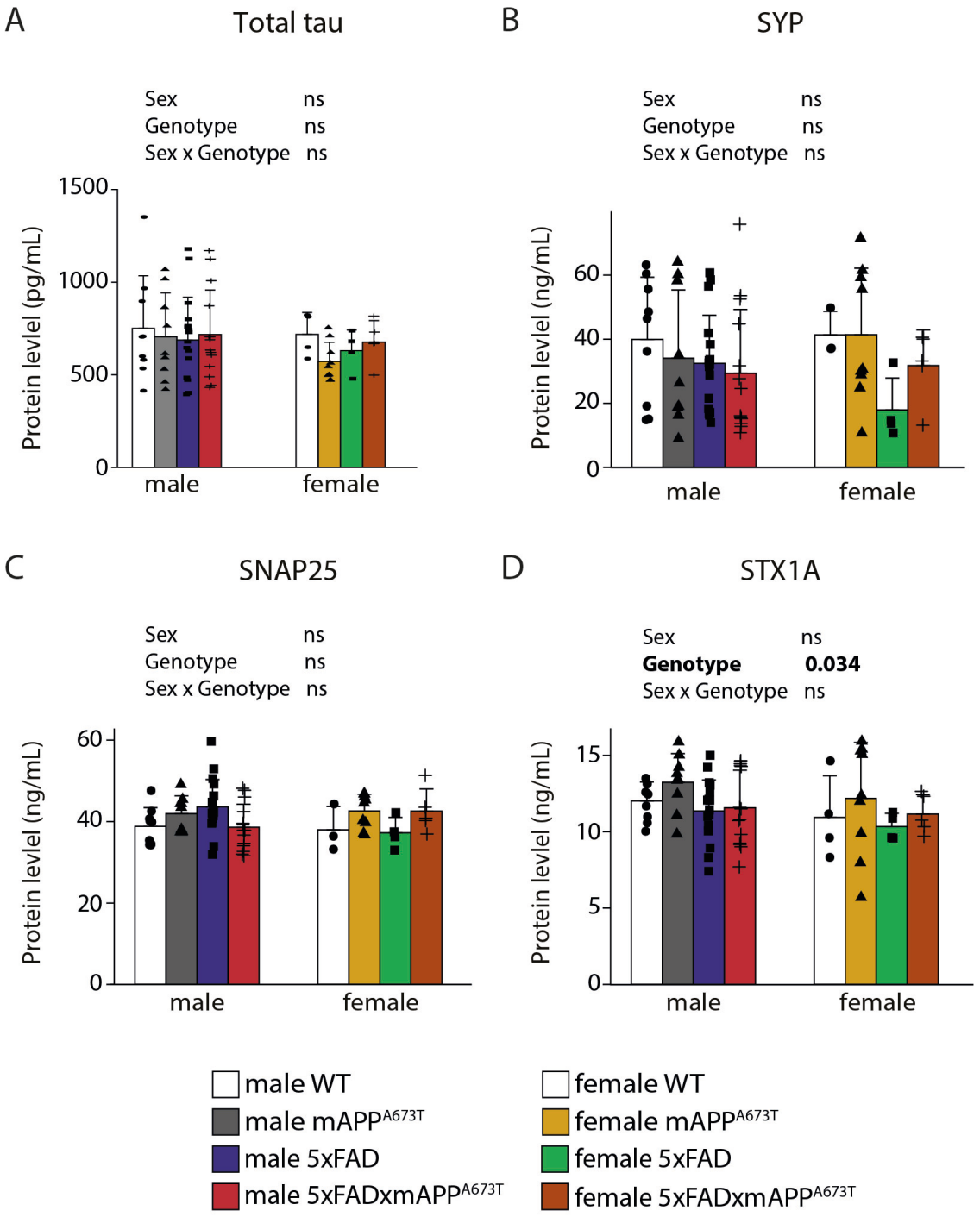

Fig. 4. Quantification of tau and synaptic proteins. (A) Mouse tau, (B) mouse synaptophysin, (C) mouse synaptosomal associated protein 25kDa, and (D) mouse syntaxin 1A were quantified in RIPA-soluble S1 fractions in male and female WT, mAPP^{A673T}, 5×FAD and 5×FAD × mAPP^{A673T} mice. Data were analysed using two-way ANOVA with sex and genotype as independent variables. Significance of each factor and the interaction is indicated above each graph. No data transformation was needed. Males: WT: n = 9, mAPP^{A673T}: n = 9, 5×FAD: n = 17, 5×FAD × mAPP^{A673T}: n = 14. Females: WT: n = 4 (SYP, SNAP25 n = 3), mAPP^{A673T}: n = 9, 5×FAD: n = 4, 5×FAD × mAPP^{A673T}: n = 5. Abbreviations: ns, not significant; SNAP25, synaptosomal associated protein 25kDa; STX1A, syntaxin 1A; SYP, synaptophysin.

significantly associated with plaque counts in females independent of genotype (Fig. 5H). The same patterns were seen when investigating the relationship between Aβ42/Aβ40 and total plaque area (**Supplementary Fig. 4**).

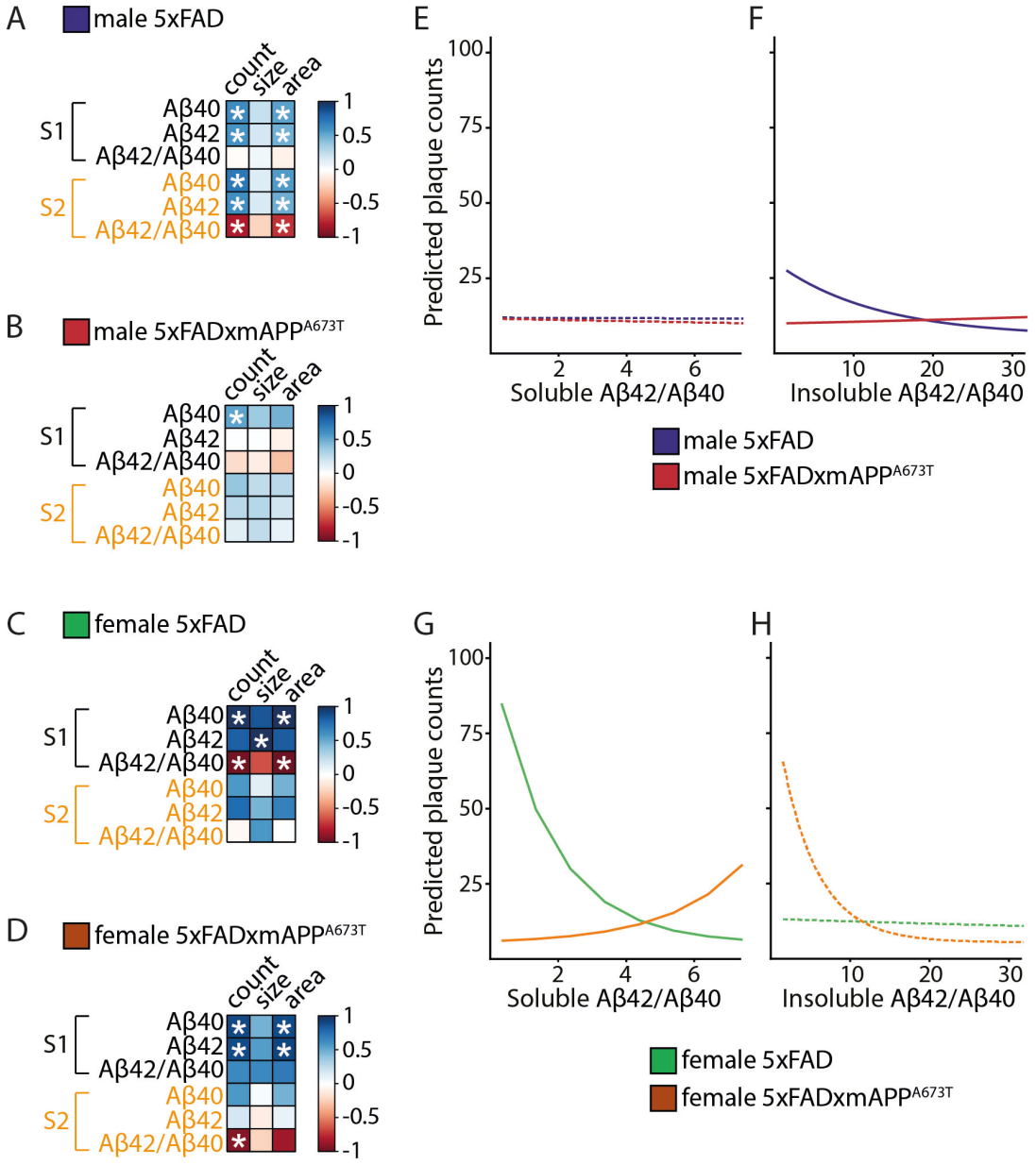

Fig. 5. Correlation matrices and linear modelling for the different Aβ measurements. (A–D) Pearson correlation matrix between Aβ40 and Aβ42 levels and their ratio (Aβ42/Aβ40) in soluble and insoluble fractions and plaque measurements (count, size, and area) are displayed for 5×FAD male (A), 5×FAD × mAPP^{A673T} male (B), 5×FAD female (C) and 5×FAD × mAPP^{A673T} female (D) mice with blue for positive correlations, red for negative correlations and white where no correlation was seen (* $p < 0.05$). Aβ levels were quantified using ELISA and plaque counts, size and total area were quantified using immunohistochemistry (averaged across brain regions). Data were analysed using Jennrich test to detect differences between matrices. (E–H) Generalized linear modelling to explore the effect of Aβ42/Aβ42 ratio in S1 and S2 on plaque counts and whether this differed across genotypes. Model-predicted plaque counts depending on Aβ42/Aβ40 ratio for 5×FAD and 5×FAD × mAPP^{A673T} male in S1 (E) and S2 (F), as well as 5×FAD and 5×FAD × mAPP^{A673T} female in S1 (G) and S2 (H) are presented. Dashed lines indicate non-significant effects.

3.4 Icelandic Mutation, Neurodegeneration, and Inflammation

Neuronal loss and gliosis associated with Aβ plaque pathologies have been reported for 5×FAD mice as early as 6 months of age [21,23]. Therefore, neurons and astrocytes were quantified in different regions of the brain using NeuN and GFAP as markers. This was done in 5×FAD, 5×FAD × mAPP^{A673T} crosses, as well as their control counterparts WT and mAPP^{A673T} (Fig. 6).

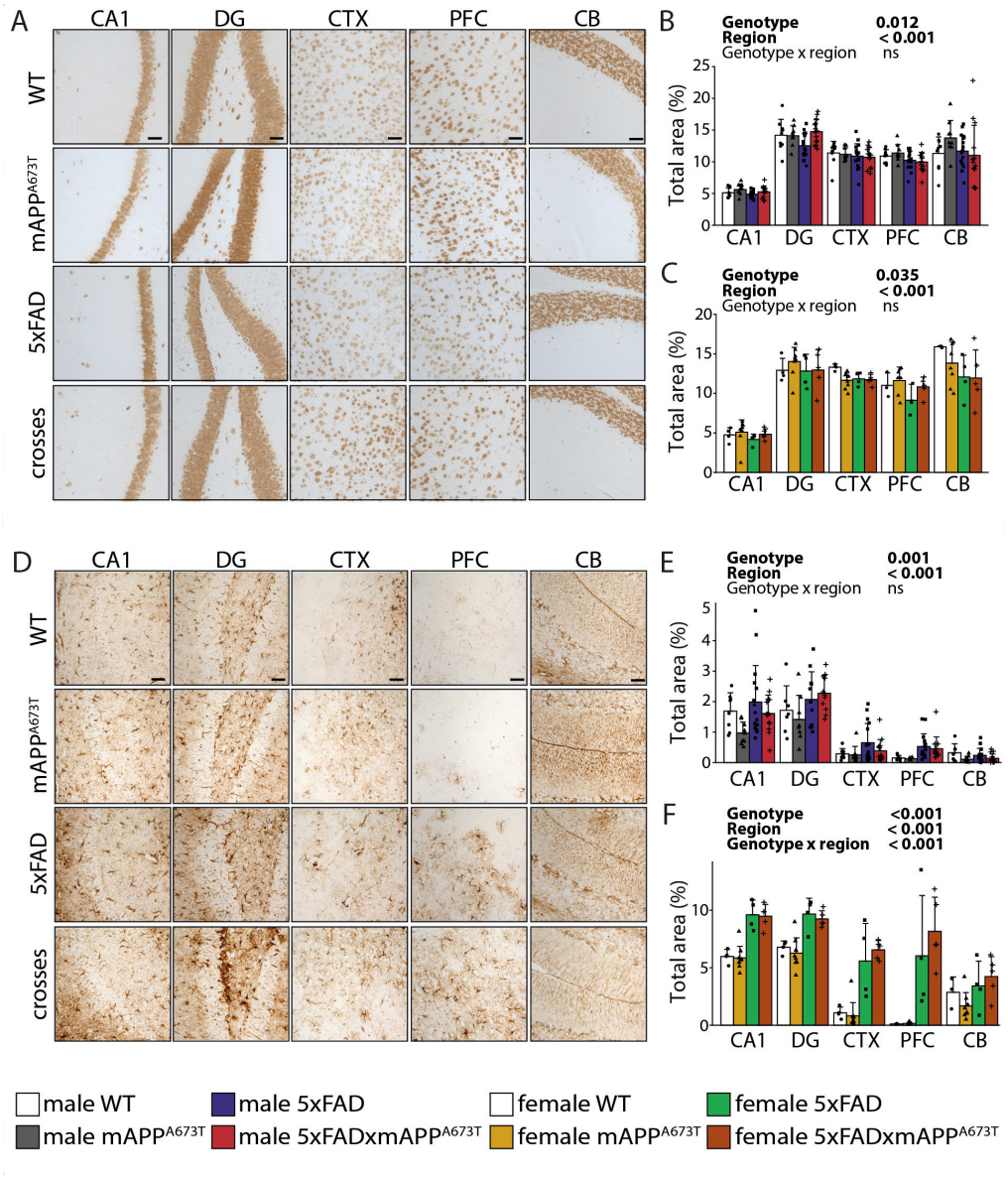

Fig. 6. NeuN and GFAP immunohistochemistry. (A) Representative NeuN immunohistochemistry images in brains of male WT, mAPP^{A673T}, 5×FAD and 5×FAD × mAPP^{A673T} mice stained with the antibody NeuN. Images from CA1, DG, CTX, PFC, and CB were taken using a light microscope at a 100× magnification. scale bars, 100 µm. NeuN levels were quantified using ilastik as total stained are in male (B) and female (C) mice in five individual brain regions. (D) Representative GFAP immunohistochemistry images in brains of male WT, mAPP^{A673T}, 5×FAD and 5×FAD × mAPP^{A673T} mice stained with the antibody GFAP. Images from CA1, DG, CTX, PFC, and CB were taken using a light microscope at a 100× magnification. scale bars, 100 µm. GFAP levels were quantified using ilastik as total stained area in male (E) and female (F) mice in five individual brain regions. Data are shown as individual values, group mean, and S.D. Statistical analysis entailed two-way ANOVA with genotype and region as independent variables. Significance of each factor and the interaction is indicated above each graph. Data were transformed using square-root transformation. NeuN - Males: WT: n = 9, mAPP^{A673T}: n = 9, 5×FAD: n = 17 (PFC n = 16), 5×FAD × mAPP^{A673T}: n = 14 (CTX and PFC n = 13). NeuN - Females: WT: n = 4 (CB and PFC n = 3), mAPP^{A673T}: n = 9 (PFC n = 7, CB n = 8), 5×FAD: n = 4 (PFC n = 3), 5×FAD × mAPP^{A673T}: n = 5. GFAP - Males: WT: n = 8 (PFC n = 6, CB, DG n = 7), mAPP^{A673T}: n = 9 (PFC n = 5, DG n = 8), 5×FAD: n = 17 (CA1, CTX n = 16, CB, PFC n = 15, DG n = 11), 5×FAD × mAPP^{A673T}: n = 14 (PFC, CTX, n = 13, DG n = 11). GFAP - Females: WT: n = 4 (CB, PFC n = 3), mAPP^{A673T}: n = 9 (CB, PFC n = 8), 5×FAD: n = 4, 5×FAD × mAPP^{A673T}: n = 5.

Representative NeuN images from CA1, DG, CTX, PFC, and CB are shown (Fig. 6A). Their quantification revealed significant genotype differences in male (Fig. 6B, $F_{Genotype}(3,222) = 3.72$, $p = 0.012$) and female cohorts

(Fig. 6C, $F_{Genotype}(3,84) = 3.00$, $p = 0.035$). In males, the average over the five brain regions confirmed the difference between the genotypes ($F_{Genotype}(3,45) = 2.30$, $p = 0.090$, data not shown) revealing a modest reduction of NeuN in 5×FAD compared to WT (–5.7%), while this reduction was even less pronounced in 5×FAD × $mAPP^{A673T}$ crosses compared to WT (–2.8%). A similar, although not significant, observation was seen in females (data not shown), where NeuN was reduced in 5×FAD compared to WT (–12.3%), and again the reduction was less pronounced in 5×FAD × $mAPP^{A673T}$ crosses compared to WT (–7.9%). Additionally, the NeuN signal differed significantly between brain regions both in male (Fig. 6B, $F_{Brain\ Region}(4,222) = 146.05$, $p < 0.001$) and female cohorts (Fig. 6C, $F_{Brain\ Region}(4,84) = 90.75$, $p < 0.001$). Post-hoc analyses yielded a lower NeuN signal in CA1 compared to all other regions in males (Fig. 6B, all p values < 0.001), and females (Fig. 6C, all p values < 0.001).

Astrocytes were labelled using GFAP (Fig. 6D), and quantification revealed genotype differences in male (Fig. 6E, $F_{Genotype}(3,194) = 9.57$, $p = 0.001$), and female cohorts (Fig. 6F, $F_{Genotype}(3,86) = 72.11$, $p < 0.001$). A significant difference between brain regions was also seen. For example, in males CA1 and DG had more GFAP-labelled astrocytes than CTX, PFC and CB (Fig. 6E, $F_{Brain\ Region}(4, 194) = 106.04$, $p < 0.001$), and similar results were observed for female cohorts (Fig. 6F, $F_{Brain\ Region}(4,86) = 54.51$, $p < 0.001$). In male mice, *post-hoc* tests revealed that $mAPP^{A673T}$ had significantly less GFAP-positive area than 5×FAD × $mAPP^{A673T}$ ($p < 0.001$) and 5×FAD ($p < 0.001$) mice. In females, *post-hoc* analysis revealed that WT and $mAPP^{A673T}$, both had less GFAP than 5×FAD and 5×FAD × $mAPP^{A673T}$ in CTX and PFC (all ps < 0.001). In male and female mice, *post-hoc* tests revealed that 5×FAD and 5×FAD × $mAPP^{A673T}$ had significantly more GFAP-positive area than WT and/or $mAPP^{A673T}$ (p values < 0.001); 5×FAD and 5×FAD × $mAPP^{A673T}$ mice, however, were not significantly different from each other.

4. Discussion

Here, we have investigated the effect of the protective Icelandic mutation, mA673T, on Aβ pathology in the 5×FAD mouse model of AD [21]. 5×FAD mice were bred with $mAPP^{A673T}$ mice resulting in 5×FAD × $mAPP^{A673T}$ crosses, that are heterozygous for both the 5×FAD mutations and the mA673T mutation in the *APP* gene. The overarching aim was to examine Aβ pathology, as well as tau and synaptic protein levels in 5×FAD and 5×FAD × $mAPP^{A673T}$ mice, including their respective WT and $mAPP^{A673T}$ controls. The main findings that we report are:

i. The $mAPP^{A673T}$ mutation significantly decreases the size of Aβ plaques in 5×FAD × $mAPP^{A673T}$ male crosses compared to 5×FAD mice.

ii. Aβ40, Aβ42 and Aβ42/Aβ40 ratios were similar between 5×FAD and 5×FAD × $mAPP^{A673T}$ crosses. However, the Icelandic mutation changed the association between Aβ42/Aβ40 plaque count/area: at low ratios, 5×FAD × $mAPP^{A673T}$ tended to show lower predicted plaque burden than 5×FAD while the opposite was true for high ratios.

iii. No differences were measured between 5×FAD and 5×FAD × $mAPP^{A673T}$ crosses for Aβ immunoblot species, tau, synaptic proteins (SYP, SNAP25, and STX1A), neuronal loss, or astrocytic gliosis.

The pathological accumulation of Aβ, either caused by its decreased clearance and/or increased oligomerisation and aggregation, leads to synaptic alterations, neuroinflammation, and eventually neuronal cell death [42]. Several aggregation-promoting mutations have been identified near the β-secretase or γ-secretase cleavage sites in the *APP* gene (amyloidogenic APP pathway), such as the Swedish K670N/M671L, Florida I716V, or London V717I mutations. A mutation with opposite effects, the Icelandic A673T mutation, has been identified in Nordic populations, and carriers of this mutation have a significantly lower risk of developing AD presumably due to increased α-secretase cleavage [18–20]. In cellular models, human A673T reduced amyloidogenic processing of human APP and decreased Aβ aggregation by reducing the release of sAPPβ [28,29]. When the human A673T was expressed in cell culture models expressing human APP with the Swedish and London mutations, it reduced sAPPβ but Aβ42, Aβ40 and the Aβ42/Aβ40 ratio remained unchanged [30] and it has also been shown in cells combining 29 FAD mutations with the human A673T mutation that the protective effect of the human A673T mutation was specific to certain mutations, e.g., the London mutation (V717I) but was absent in the Florida (I716V) and Swedish (KM670/671NL) mutations [43]. It was therefore reasonable to hypothesise that the Icelandic mutation in the murine *APP* gene, mA673T, could counteract, at least in part, some of the effects introduced by the Swedish/Florida/London mutations in terms of Aβ and other pathologies in 5×FAD mice, especially because it has been suggested that endogenous mouse Aβ may alter human Aβ in transgenic models [34].

4.1 Icelandic Mutation and Aβ

Histopathologically, the mA673T mutation led to a decrease in Aβ plaque size in 5×FAD × $mAPP^{A673T}$ males compared to 5×FAD. While both Aβ40 and Aβ42 are found in plaques, however an increased cerebral Aβ42/Aβ40 ratio is another well-established biomarker of Aβ pathology in patients and 5×FAD mice, due to the greater aggregation propensity of Aβ42 [44,45]. While no overt differences were identified for soluble/insoluble Aβ40 and Aβ42, we found the way in which their ratio was associated with plaques differed considerably between 5×FAD and 5×FAD

× mAPP^{A673T}; male 5×FAD mice showed significant positive correlations between insoluble Aβ40 and Aβ42 with plaque counts and area. These were almost entirely absent in 5×FAD × mAPP^{A673T}. Similarly, in females with heightened soluble and insoluble Aβ40 and Aβ42 levels ([25], this study), the Aβ42/Aβ40 ratio in soluble fractions correlated significantly with plaque count/area in 5×FAD mice, but this was not the case in 5×FAD × mAPP^{A673T}. When modelling these, genotype-differences depended on Aβ42/Aβ40 ratios; a protective effect (i.e., reduced plaque burden in 5×FAD × mAPP^{A673T}) was seen at low ratios that disappeared or is reversed at high ratios. These differences suggest a genotype-dependent sensitivity to Aβ accumulation. They would also suggest the strength of the amyloid burden in 5×FAD mice is too aggressive and the protection is too weak to counteract their aggregation propensity.

Only a few publications have addressed the potential protective effects of the Icelandic mutation in AD models *in vivo*. The first used a knock-in rat model of humanized A673T-APP, K670N/M671L-APP (Swedish mutation) or both, and found a reduction of Aβ40 and Aβ42 pathology (using ELISA) for A673T-APP compared to wild-type APP but not when the Icelandic mutation was combined with the Swedish mutation [33]. Using immunoblotting, they corroborated an increase in non-amyloidogenic APP metabolites (sAPPα) and a decrease in amyloidogenic APP metabolites (sAPPβ and βCTF) again for the Icelandic mutation alone, but not when combined with the Swedish mutation. The authors suggested that the Swedish and Icelandic mutations may act independently but the magnitude of the protective effect caused by the Icelandic mutation is smaller than the aggressive pathogenic effect of the Swedish mutation. We have found no differences in APP fragments between genotypes using immunoblotting, confirming a lack of efficacy of mA673T when combined with the Swedish mutation and suggesting no shift in APP processing in 5×FAD mice when the mA673T mutation is introduced on a Swedish/Florida/London background. The second study generated knock-in mice with humanized APP with the Arctic (E693B) and Beyreuther/Iberian (I715F) mutations and compared them to mice also carrying the Icelandic mutation [32]. The protective A673T mutation reduced plaque area in cortex and hippocampus at 8 months of age but at 12 months, only the number of plaques larger than 20 µm was decreased while smaller plaques showed similar levels in both genotypes. They additionally report a decrease in βCTF at 3 months (where no Aβ pathology is established yet) but it is unclear if this persists at older age, where we also could not see any shift in APP processing. In our male 5×FAD × mAPP^{A673T} mice, only the plaque size was decreased compared to 5×FAD, suggesting a more aggressive Aβ pathology produced by the Swedish/Florida/London mutations as compared to the Arctic or Beyreuther/Iberian APP mutations. This is also supported by *in vitro* findings, where it has been shown that the protective effect of the human A673T mutation was specific to the London mutation (V717I) but was absent in the Florida (I716V) and Swedish (KM670/671NL) mutations [30,43]. Another study inoculated APPswe/PS1dE9 transgenic mice with either recombinant non-mutant human Aβ or human Aβ containing the A673T mutation once at 2 months of age and found no changes in Aβ levels when analysed at 6 months. There was only a rescue in synapse density and spatial memory which remained unexplained [31]. In this model, similar to our 5×FAD mouse, the role of PS1 mutations remain unexplored and individual contributions of these mutations to the amyloid load, and a possible block of the A673T protection are elusive to date. Lastly, a recent study that introduced the mA673T mutation into a tau-transgenic model, L66, reported no modulation of mouse Aβ or human tau pathologies and no rescue of motor and neuropsychiatric behaviour in these mice [46].

5×FAD mice overexpress randomly integrated mutant human Aβ, while in mAPP^{A673T} mice, the Icelandic A673T mutation was generated in the murine *APP* gene. It has been shown that co-expression of murine APP can alter Aβ pathology in APP23 transgenic mice but not in the much faster Aβ-depositing APPPS1 transgenic mice [34]. Moreover, the targeted knock-in of human BACE1 lead to amyloidosis purely based on murine Aβ [47]. On the contrary, Jankowsky and co-workers showed that overexpression of mouse APP did not alter Aβ pathology when expressed on a PS1dE9 background, while it increased Aβ pathology when expressed on a more aggressive APPswe/PS1dE9 background [48]. These data suggest a differential effect of murine Aβ on human Aβ deposition in the different APP mouse models and may explain the mild effects observed in this study.

4.2 Icelandic Mutation and Tau

Several lines of evidence suggest a connection between Aβ and tau in the pathophysiology of AD, with both proteins being abundant and often co-localising at synapses [49–53]. It is therefore important to quantify tau levels to confirm if they are affected by APP alterations. A study investigating the effect of the Icelandic mutation in an APP/PS1 mouse model of AD reported a decrease in phospho-tau pathology in the A673T-Aβ groups, but this reduction remains unexplained [31]. By contrast, the mA673T mutation did not affect tau levels and was unable to rescue behavioural impairment in a tau-transgenic mouse model [46]. A recent exploratory study in 6 non-AD patients (unconfirmed idiopathic normal pressure hydrocephalus cases) comparing CSF of three APP^{A673T} carriers to three age- (and sex-) matched control subjects reported that disease-relevant soluble APP-β and Aβ42 levels were significantly reduced in the CSF of APP^{A673T} carries. Yet, soluble APP-α, total tau and phosphorylated tau (p-tau 181) were not altered [30]. This is in line with our finding that the Icelandic mutation had no effect on tau, as 5×FAD

and 5×FAD × mAPP^{A673T} mice presented with similar tau levels. It is worth mentioning that 5×FAD showed normal tau levels not dissimilar of WT mice and is in line with unchanged total tau levels in 5×FAD compared to WT at 3 months of age [54].

4.3 Icelandic Mutation and Synaptic Proteins

Synapse loss is a key event in AD that strongly correlates with cognitive decline [55,56]. Additionally, a link between Aβ plaque formation and synaptic dysfunction has been established [57]. The presynaptic proteins SYP and SNAP25 were chosen as established markers for synapse loss in AD and AD mouse models, while STX1A was chosen as negative, non-changing, marker [26,55,58]. The expression of the mAPP^{A673T} mutation in 5×FAD did not alter levels of these three synaptic markers, in line with a recent report investigating the exact same mutation in a tau-based animal model [46]. However, they also were unchanged across all genotypes despite previous reports of a general reduction of synaptic proteins in 5×FAD as early as 6 months [26], most notably a reduction between 30 and 45% for SYP [59–61]. These discrepancies likely relate to the different quantification methods used (immunoblotting/immunofluorescence vs. ELISA).

4.4 Icelandic Mutation, Neurodegeneration, and Inflammation

Neuronal loss is a further key pathological feature of neurodegenerative disease such as AD [62]. Conflicting findings were reported for neuronal loss in 5×FAD mice. On one hand, stereologically counted neuron numbers were lower in cortical layer 5 starting at 9 months [63] and persisted at 12 months [23], while on the other neuronal loss appeared as early as 6 months in the subiculum [64]. Our analyses based on area stained in microscopic images using the ilastik software returned no significant changes of the NeuN staining in 5×FAD mice in any of the five brain regions analysed, and no effect of the mA673T mutation. Contrary, more GFAP-positive astrocytes were found for in 5×FAD mice, but no protective effect was observed in 5×FAD × mAPP^{A673T} crosses.

5. Conclusions

Collectively, we here show that the Icelandic mutation in the murine *APP* gene, mA673T, has only moderate effects on Aβ pathology in 5×FAD mice, which is likely due to the aggressive Aβ pathology evoked at 6-month of age by the combination of the Swedish, Florida and London APP, and PS1 mutations.

Disclosure

The paper is listed as, "The Icelandic mutation APPA673T on amyloid-β plaque burden in the 5×FAD Alzheimer model" as a preprint on (Biorxiv) at: https://www.biorxiv.org/content/10.1101/2025.11.05.686739v1.

Abbreviations

5×FAD, five familial Alzheimer's disease mice; 5×FAD × mAPP^{A673T}, mouse crosses carrying both the 5×FAD mutations and the A673T mutation in the murine *APP* gene; Aβ, amyloid beta-protein; AD, Alzheimer's disease; AEBSF, 4-(2-aminoethyl) benzenesulfonyl fluoride hydrochloride; APP, amyloid precursor protein; mAPP^{A673T}, mice with the A673T Icelandic mutation in the murine *APP* gene; BCA, bicinchoninic acid; CA1, hippocampal cornu ammonis; CB, cerebellum; CTF, carboxyl terminal fragment; CTX, visual cortex; DG, dentate gyrus; GFAP, glial fibrillary acidic protein; GuHCl, guanidine hydrochloride; IHC, immunohistochemistry; NeuN, neuronal nuclear antigen; PFC, prefrontal cortex; PS1, presenilin-1; S.D., standard deviation; S1, RIPA-soluble supernatant fraction; S2, GuHCl fraction or RIPA-insoluble fraction; SNAP25, synaptosome associated protein 25kDa; STX1A, syntaxin 1A; SYP, synaptophysin; WT, C57Bl6/J wild-type mice.

Availability of Data and Materials

Data will be made available on reasonable request.

Author Contributions

AA: Investigation, Data curation, Formal analysis, Visualization, Writing — Original Draft; RL: Investigation; TV: Investigation; BP: Conceptualization, Resources, Writing — Review & Editing; CRH: Conceptualization, Writing — Review & Editing, Funding acquisition; GR: Conceptualization, Supervision, Project administration, Funding acquisition, Writing — Review & Editing; KS: Conceptualization, Supervision, Investigation, Data curation, Formal analysis, Visualization, Writing — Original Draft. All authors contributed to editorial changes in the manuscript. All authors read and approved the final manuscript. All authors have participated sufficiently in the work and agreed to be accountable for all aspects of the work.

Ethics Approval and Consent to Participate

All animal experiments were performed in accordance with the European Communities Council Directive (63/2010/EU) and a project licence with University of Aberdeen Animal Welfare and Ethical Review Body (AWERB) (approval number: PP2213334) under the UK Animals (Scientific Procedures) Act (1986) and its Amended Regulations (2012) and complied with the ARRIVE 2.0 guidelines. No human samples were used in this study.

Acknowledgment

The authors acknowledge Drs. Lianne Robinson and Valeria Melis for support with animal perfusions, and Dariia Babych for support with ELISA.

Funding

This work was funded by TauRx Therapeutics Ltd., Singapore (PAR1577 and PAR2074).

Conflict of Interest

CRH holds an Office with TauRx Therapeutics Ltd. All authors declare no conflicts of interest. Despite they received sponsorship from TauRx Therapeutics Ltd., the judgments in data interpretation and writing were not influenced by this relationship. Gernot Riedel is serving as one of the Editorial Board members of this journal. Bettina Platt is serving as the Editor in chief of this journal. We declare that Gernot Riedel and Bettina Platt had no involvement in the peer review of this article and has no access to information regarding its peer review. Full responsibility for the editorial process for this article was delegated to Andrei Surguchov.

Supplementary Material

Supplementary material associated with this article can be found, in the online version, at https://doi.org/10.31083/JIN48581.

References

[1] Scott KR, Barrett AM. Dementia syndromes: evaluation and treatment. Expert Review of Neurotherapeutics. 2007; 7: 407–422. https://doi.org/10.1586/14737175.7.4.407.

[2] GBD 2019 Dementia Forecasting Collaborators. Estimation of the global prevalence of dementia in 2019 and forecasted prevalence in 2050: an analysis for the Global Burden of Disease Study 2019. The Lancet. Public Health. 2022; 7: e105–e125. https://doi.org/10.1016/S2468-2667(21)00249-8.

[3] Alzheimer A. Uber eine eigenartige Erkrankung der Hirnrinde. Allgemeine Zeitschrift Fur Psychiatrie Und Psychischgerichtliche Medizin 1907; 64: 146–148. (In German)

[4] Zhang H, Wei W, Zhao M, Ma L, Jiang X, Pei H, *et al*. Interaction between Aβ and Tau in the Pathogenesis of Alzheimer's Disease. International Journal of Biological Sciences. 2021; 17: 2181–2192. https://doi.org/10.7150/ijbs.57078.

[5] Cho Y, Bae HG, Okun E, Arumugam TV, Jo DG. Physiology and pharmacology of amyloid precursor protein. Pharmacology & Therapeutics. 2022; 235: 108122. https://doi.org/10.1016/j.pharmthera.2022.108122.

[6] Gabriele RMC, Abel E, Fox NC, Wray S, Arber C. Knockdown of Amyloid Precursor Protein: Biological Consequences and Clinical Opportunities. Frontiers in Neuroscience. 2022; 16: 835645. https://doi.org/10.3389/fnins.2022.835645.

[7] Bitan G, Kirkitadze MD, Lomakin A, Vollers SS, Benedek GB, Teplow DB. Amyloid beta -protein (Abeta) assembly: Abeta 40 and Abeta 42 oligomerize through distinct pathways. Proceedings of the National Academy of Sciences of the United States of America. 2003; 100: 330–335. https://doi.org/10.1073/pnas.222681699.

[8] Golde TE, Eckman CB, Younkin SG. Biochemical detection of Abeta isoforms: implications for pathogenesis, diagnosis, and treatment of Alzheimer's disease. Biochimica et Biophysica Acta. 2000; 1502: 172–187. https://doi.org/10.1016/s0925-4439(00)00043-0.

[9] Kuperstein I, Broersen K, Benilova I, Rozenski J, Jonckheere W, Debulpaep M, *et al*. Neurotoxicity of Alzheimer's disease Aβ peptides is induced by small changes in the Aβ42 to Aβ40 ratio. The EMBO Journal. 2010; 29: 3408–3420. https://doi.org/10.1038/emboj.2010.211.

[10] Scheuner D, Eckman C, Jensen M, Song X, Citron M, Suzuki N, *et al*. Secreted amyloid beta-protein similar to that in the senile plaques of Alzheimer's disease is increased in vivo by the presenilin 1 and 2 and APP mutations linked to familial Alzheimer's disease. Nature Medicine. 1996; 2: 864–870. https://doi.org/10.1038/nm0896-864.

[11] Cras P, Kawai M, Lowery D, Gonzalez-DeWhitt P, Greenberg B, Perry G. Senile plaque neurites in Alzheimer disease accumulate amyloid precursor protein. Proceedings of the National Academy of Sciences of the United States of America. 1991; 88: 7552–7556. https://doi.org/10.1073/pnas.88.17.7552.

[12] Eanes ED, Glenner GG. X-ray diffraction studies on amyloid filaments. The Journal of Histochemistry and Cytochemistry: Official Journal of the Histochemistry Society. 1968; 16: 673–677. https://doi.org/10.1177/16.11.673.

[13] Glenner GG, Wong CW. Alzheimer's disease: initial report of the purification and characterization of a novel cerebrovascular amyloid protein. Biochemical and Biophysical Research Communications. 1984; 120: 885–890. https://doi.org/10.1016/s0006-291x(84)80190-4.

[14] Glenner GG, Wong CW. Alzheimer's disease and Down's syndrome: sharing of a unique cerebrovascular amyloid fibril protein. Biochemical and Biophysical Research Communications. 1984; 122: 1131–1135. https://doi.org/10.1016/0006-291x(84)91209-9.

[15] Kang J, Lemaire HG, Unterbeck A, Salbaum JM, Masters CL, Grzeschik KH, *et al*. The precursor of Alzheimer's disease amyloid A4 protein resembles a cell-surface receptor. Nature. 1987; 325: 733–736. https://doi.org/10.1038/325733a0.

[16] Masters CL, Simms G, Weinman NA, Multhaup G, McDonald BL, Beyreuther K. Amyloid plaque core protein in Alzheimer disease and Down syndrome. Proceedings of the National Academy of Sciences of the United States of America. 1985; 82: 4245–4249. https://doi.org/10.1073/pnas.82.12.4245.

[17] Tcw J, Goate AM. Genetics of β-Amyloid Precursor Protein in Alzheimer's Disease. Cold Spring Harbor Perspectives in Medicine. 2017; 7: a024539. https://doi.org/10.1101/cshperspect.a024539.

[18] Jonsson T, Atwal JK, Steinberg S, Snaedal J, Jonsson PV, Bjornsson S, *et al*. A mutation in APP protects against Alzheimer's disease and age-related cognitive decline. Nature. 2012; 488: 96–99. https://doi.org/10.1038/nature11283.

[19] Martiskainen H, Herukka SK, Stančáková A, Paananen J, Soininen H, Kuusisto J, *et al*. Decreased plasma β-amyloid in the Alzheimer's disease APP A673T variant carriers. Annals of Neurology. 2017; 82: 128–132. https://doi.org/10.1002/ana.24969.

[20] Xia Q, Yang X, Shi J, Liu Z, Peng Y, Wang W, *et al*. The Protective A673T Mutation of Amyloid Precursor Protein (APP) in Alzheimer's Disease. Molecular Neurobiology. 2021; 58: 4038–4050. https://doi.org/10.1007/s12035-021-02385-y.

[21] Oakley H, Cole SL, Logan S, Maus E, Shao P, Craft J, *et al*. Intraneuronal beta-amyloid aggregates, neurodegeneration, and neuron loss in transgenic mice with five familial Alzheimer's disease mutations: potential factors in amyloid plaque formation. The Journal of Neuroscience: the Official Journal of the Society for Neuroscience. 2006; 26: 10129–10140. https://doi.org/10.1523/JNEUROSCI.1202-06.2006.

[22] Forner S, Kawauchi S, Balderrama-Gutierrez G, Kramár EA, Matheos DP, Phan J, *et al*. Systematic phenotyping and characterization of the 5xFAD mouse model of Alzheimer's disease. Scientific Data. 2021; 8: 270. https://doi.org/10.1038/s41597-021-01054-y.

[23] Jawhar S, Trawicka A, Jenneckens C, Bayer TA, Wirths O. Mo-

tor deficits, neuron loss, and reduced anxiety coinciding with axonal degeneration and intraneuronal Aβ aggregation in the 5XFAD mouse model of Alzheimer's disease. Neurobiology of Aging. 2012; 33: 196.e29–40. https://doi.org/10.1016/j.neurobiolaging.2010.05.027.

[24] Oblak AL, Lin PB, Kotredes KP, Pandey RS, Garceau D, Williams HM, *et al*. Comprehensive Evaluation of the 5XFAD Mouse Model for Preclinical Testing Applications: A MODEL-AD Study. Frontiers in Aging Neuroscience. 2021; 13: 713726. https://doi.org/10.3389/fnagi.2021.713726.

[25] Sil A, Erfani A, Lamb N, Copland R, Riedel G, Platt B. Sex Differences in Behavior and Molecular Pathology in the 5XFAD Model. Journal of Alzheimer's Disease: JAD. 2022; 85: 755–778. https://doi.org/10.3233/JAD-210523.

[26] Anschuetz A, Schwab K, Harrington CR, Wischik CM, Riedel G. Proteomic and non-proteomic changes of presynaptic proteins in animal models of Alzheimer's disease: A meta-analysis 2015-2023. Journal of Alzheimer's Disease: JAD. 2025; 107: 452–476. https://doi.org/10.1177/13872877251362212.

[27] Jang H, Lee S, Kim YJ, Lee J, Kim SW, Son Y, *et al*. Progressive Hippocampal Neuroarchitecture Changes in the 5×FAD Alzheimer's Disease Mouse Model. Journal of Integrative Neuroscience. 2025; 24: 40831. https://doi.org/10.31083/JIN40831.

[28] Kokawa A, Ishihara S, Fujiwara H, Nobuhara M, Iwata M, Ihara Y, *et al*. The A673T mutation in the amyloid precursor protein reduces the production of β-amyloid protein from its β-carboxyl terminal fragment in cells. Acta Neuropathologica Communications. 2015; 3: 66. https://doi.org/10.1186/s40478-015-0247-6.

[29] Maloney JA, Bainbridge T, Gustafson A, Zhang S, Kyauk R, Steiner P, *et al*. Molecular mechanisms of Alzheimer disease protection by the A673T allele of amyloid precursor protein. The Journal of Biological Chemistry. 2014; 289: 30990–31000. https://doi.org/10.1074/jbc.M114.589069.

[30] Wittrahm R, Takalo M, Kuulasmaa T, Mäkinen PM, Mäkinen P, Končarević S, *et al*. Protective Alzheimer's disease-associated APP A673T variant predominantly decreases sAPPβ levels in cerebrospinal fluid and 2D/3D cell culture models. Neurobiology of Disease. 2023; 182: 106140. https://doi.org/10.1016/j.nbd.2023.106140.

[31] Célestine M, Jacquier-Sarlin M, Borel E, Petit F, Lante F, Bousset L, *et al*. Transmissible long-term neuroprotective and pro-cognitive effects of 1-42 beta-amyloid with A2T icelandic mutation in an Alzheimer's disease mouse model. Molecular Psychiatry. 2024; 29: 3707–3721. https://doi.org/10.1038/s41380-024-02611-8.

[32] Shimohama S, Fujioka R, Mihira N, Sekiguchi M, Sartori L, Joho D, *et al*. The Icelandic Mutation (APP-A673T) Is Protective against Amyloid Pathology In Vivo. The Journal of Neuroscience: the Official Journal of the Society for Neuroscience. 2024; 44: e0223242024. https://doi.org/10.1523/JNEUROSCI.0223-24.2024.

[33] Tambini MD, Norris KA, D'Adamio L. Opposite changes in APP processing and human Aβ levels in rats carrying either a protective or a pathogenic APP mutation. eLife. 2020; 9: e52612. https://doi.org/10.7554/eLife.52612.

[34] Mahler J, Morales-Corraliza J, Stolz J, Skodras A, Radde R, Duma CC, *et al*. Endogenous murine Aβ increases amyloid deposition in APP23 but not in APPPS1 transgenic mice. Neurobiology of Aging. 2015; 36: 2241–2247. https://doi.org/10.1016/j.neurobiolaging.2015.03.011.

[35] Percie du Sert N, Hurst V, Ahluwalia A, Alam S, Avey MT, Baker M, *et al*. The ARRIVE guidelines 2.0: Updated guidelines for reporting animal research. Journal of Cerebral Blood Flow and Metabolism: Official Journal of the International Society of Cerebral Blood Flow and Metabolism. 2020; 40: 1769–1777. https://doi.org/10.1177/0271678X20943823.

[36] Paxinos G, Franklin K. The Mouse Brain in Stereotaxic Coordinates. 5th edn. Academic Press: Cambridge, Massachusetts, USA. 2019.

[37] Lemke N, Melis V, Lauer D, Magbagbeolu M, Neumann B, Harrington CR, *et al*. Differential compartmental processing and phosphorylation of pathogenic human tau and native mouse tau in the line 66 model of frontotemporal dementia. The Journal of Biological Chemistry. 2020; 295: 18508–18523. https://doi.org/10.1074/jbc.RA120.014890.

[38] Berg S, Kutra D, Kroeger T, Straehle CN, Kausler BX, Haubold C, *et al*. ilastik: interactive machine learning for (bio)image analysis. Nature Methods. 2019; 16: 1226–1232. https://doi.org/10.1038/s41592-019-0582-9.

[39] Schindelin J, Arganda-Carreras I, Frise E, Kaynig V, Longair M, Pietzsch T, *et al*. Fiji: an open-source platform for biological-image analysis. Nature Methods. 2012; 9: 676–682. https://doi.org/10.1038/nmeth.2019.

[40] Jennrich RI. An Asymptotic $\chi 2$ Test for the Equality of Two Correlation Matrices. Journal of the American Statistical Association. 1970; 65: 904–912. https://doi.org/10.1080/01621459.1970.10481133.

[41] Serneels L, T'Syen D, Perez-Benito L, Theys T, Holt MG, De Strooper B. Modeling the β-secretase cleavage site and humanizing amyloid-beta precursor protein in rat and mouse to study Alzheimer's disease. Molecular Neurodegeneration. 2020; 15: 60. https://doi.org/10.1186/s13024-020-00399-z.

[42] Hampel H, Hardy J, Blennow K, Chen C, Perry G, Kim SH, *et al*. The Amyloid-β Pathway in Alzheimer's Disease. Molecular Psychiatry. 2021; 26: 5481–5503. https://doi.org/10.1038/s41380-021-01249-0.

[43] Guyon A, Rousseau J, Lamothe G, Tremblay JP. The protective mutation A673T in amyloid precursor protein gene decreases Aβ peptides production for 14 forms of Familial Alzheimer's Disease in SH-SY5Y cells. PloS One. 2020; 15: e0237122. https://doi.org/10.1371/journal.pone.0237122.

[44] Andersson E, Lindblom N, Janelidze S, Salvadó G, Gkanatsiou E, Söderberg L, *et al*. Soluble cerebral Aβ protofibrils link Aβ plaque pathology to changes in CSF Aβ_{42}/Aβ_{40} ratios, neurofilament light and tau in Alzheimer's disease model mice. Nature Aging. 2025; 5: 366–375. https://doi.org/10.1038/s43587-025-00810-8.

[45] Blennow K, Zetterberg H. Biomarkers for Alzheimer's disease: current status and prospects for the future. Journal of Internal Medicine. 2018; 284: 643–663. https://doi.org/10.1111/joim.12816.

[46] Anschuetz A, Robinson L, Mondesir M, Melis V, Platt B, Harrington CR, *et al*. The effect of the Icelandic mutation APPA673T in the line 66 model of tauopathy. Biomolecules. 2026; 16: 28 https://doi.org/10.3390/biom16010028.

[47] Plucińska K, Crouch B, Koss D, Robinson L, Siebrecht M, Riedel G, *et al*. Knock-in of human BACE1 cleaves murine APP and reiterates Alzheimer-like phenotypes. The Journal of Neuroscience: the Official Journal of the Society for Neuroscience. 2014; 34: 10710–10728. https://doi.org/10.1523/JNEUROSCI.0433-14.2014.

[48] Jankowsky JL, Younkin LH, Gonzales V, Fadale DJ, Slunt HH, Lester HA, *et al*. Rodent A beta modulates the solubility and distribution of amyloid deposits in transgenic mice. The Journal of Biological Chemistry. 2007; 282: 22707–22720. https://doi.org/10.1074/jbc.M611050200.

[49] Fein JA, Sokolow S, Miller CA, Vinters HV, Yang F, Cole GM, *et al*. Co-localization of amyloid beta and tau pathology in Alzheimer's disease synaptosomes. The American Journal of Pathology. 2008; 172: 1683–1692. https://doi.org/10.2353/ajpath.2008.070829.

[50] Henkins KM, Sokolow S, Miller CA, Vinters HV, Poon WW,

Cornwell LB, *et al*. Extensive p-tau pathology and SDS-stable p-tau oligomers in Alzheimer's cortical synapses. Brain Pathology (Zurich, Switzerland). 2012; 22: 826–833. https://doi.org/10.1111/j.1750-3639.2012.00598.x.

[51] Kurucu H, Colom-Cadena M, Davies C, Wilkins L, King D, Rose J, *et al*. Inhibitory synapse loss and accumulation of amyloid beta in inhibitory presynaptic terminals in Alzheimer's disease. European Journal of Neurology. 2022; 29: 1311–1323. https://doi.org/10.1111/ene.15043.

[52] Sokolow S, Luu SH, Nandy K, Miller CA, Vinters HV, Poon WW, *et al*. Preferential accumulation of amyloid-beta in presynaptic glutamatergic terminals (VGluT1 and VGluT2) in Alzheimer's disease cortex. Neurobiology of Disease. 2012; 45: 381–387. https://doi.org/10.1016/j.nbd.2011.08.027.

[53] Tai HC, Wang BY, Serrano-Pozo A, Frosch MP, Spires-Jones TL, Hyman BT. Frequent and symmetric deposition of misfolded tau oligomers within presynaptic and postsynaptic terminals in Alzheimer's disease. Acta Neuropathologica Communications. 2014; 2: 146. https://doi.org/10.1186/s40478-014-0146-2.

[54] Héraud C, Goufak D, Ando K, Leroy K, Suain V, Yilmaz Z, *et al*. Increased misfolding and truncation of tau in APP/PS1/tau transgenic mice compared to mutant tau mice. Neurobiology of Disease. 2014; 62: 100–112. https://doi.org/10.1016/j.nbd.2013.09.010.

[55] de Wilde MC, Overk CR, Sijben JW, Masliah E. Meta-analysis of synaptic pathology in Alzheimer's disease reveals selective molecular vesicular machinery vulnerability. Alzheimer's & Dementia: the Journal of the Alzheimer's Association. 2016; 12: 633–644. https://doi.org/10.1016/j.jalz.2015.12.005.

[56] Spires-Jones TL, Hyman BT. The intersection of amyloid beta and tau at synapses in Alzheimer's disease. Neuron. 2014; 82: 756–771. https://doi.org/10.1016/j.neuron.2014.05.004.

[57] Zhang H, Jiang X, Ma L, Wei W, Li Z, Chang S, *et al*. Role of Aβ in Alzheimer's-related synaptic dysfunction. Frontiers in Cell and Developmental Biology. 2022; 10: 964075. https://doi.org/10.3389/fcell.2022.964075.

[58] Anschuetz A, Schwab K, Harrington CR, Wischik CM, Riedel G. A Meta-Analysis on Presynaptic Changes in Alzheimer's Disease. Journal of Alzheimer's Disease: JAD. 2024; 97: 145–162. https://doi.org/10.3233/JAD-231034.

[59] Jiang LX, Huang GD, Su F, Wang H, Zhang C, Yu X. Vortioxetine administration attenuates cognitive and synaptic deficits in 5×FAD mice. Psychopharmacology. 2020; 237: 1233–1243. https://doi.org/10.1007/s00213-020-05452-9.

[60] Kim J, Kang S, Chang KA. Effect of cx-DHED on Abnormal Glucose Transporter Expression Induced by AD Pathologies in the 5xFAD Mouse Model. International Journal of Molecular Sciences. 2022; 23: 10602. https://doi.org/10.3390/ijms231810602.

[61] Vasilopoulou F, Rodríguez-Arévalo S, Bagán A, Escolano C, Griñán-Ferré C, Pallàs M. Disease-modifying treatment with I_2 imidazoline receptor ligand LSL60101 in an Alzheimer's disease mouse model: a comparative study with donepezil. British Journal of Pharmacology. 2021; 178: 3017–3033. https://doi.org/10.1111/bph.15478.

[62] Crews L, Masliah E. Molecular mechanisms of neurodegeneration in Alzheimer's disease. Human Molecular Genetics. 2010; 19: R12–R20. https://doi.org/10.1093/hmg/ddq160.

[63] Eimer WA, Vassar R. Neuron loss in the 5XFAD mouse model of Alzheimer's disease correlates with intraneuronal Aβ42 accumulation and Caspase-3 activation. Molecular Neurodegeneration. 2013; 8: 2. https://doi.org/10.1186/1750-1326-8-2.

[64] Poon CH, Wong STN, Roy J, Wang Y, Chan HWH, Steinbusch H, *et al*. Sex Differences between Neuronal Loss and the Early Onset of Amyloid Deposits and Behavioral Consequences in 5xFAD Transgenic Mouse as a Model for Alzheimer's Disease. Cells. 2023; 12: 780. https://doi.org/10.3390/cells12050780.